19th International Conference on
Adaptive Structures and Technologies
October 6-9, 2008
Ascona, Switzerland

Intelligent Tires Using Strain Measurement For Improved Tire Safety

Ryosuke Matsuzaki[1]* and Akira Todoroki[1]
[1] Department of Mechanical Sciences and Engineering, Tokyo Institute of Technology, Japan
*2-12-1-I1-66, Ookayama, Meguro, Tokyo, Japan. Tel/Fax: +81-3-5734-3184, Mail: rmatsuza@ginza.mes.titech.ac.jp

ABSTRACT

From a traffic safety point-of-view, there is an urgent need for intelligent tires as a warning system for road conditions, for optimized braking control on poor road surfaces and as a tire fault detection system. Intelligent tires, equipped with sensors for monitoring applied strain, are effective in improving reliability and control systems such as anti-lock braking systems (ABSs). In previous studies, we developed a direct tire deformation or strain measurement system with sufficiently low stiffness and high elongation for practical use, and a wireless communication system between tires and vehicle that operates without a battery. The present study investigates the application of strain data for an optimized braking control and road condition warning system. The relationships between strain sensor outputs and tire mechanical parameters, including braking torque, effective radius and contact patch length, are calculated using finite element analysis. Finally, we suggested the possibility of optimized braking control and road condition warning systems. Optimized braking control can be achieved by keeping the slip ratio constant. The road condition warning would be actuated if the recorded friction coefficient at a certain slip ratio is lower than a 'safe' reference value.

Keywords: Intelligent tires, Strain monitoring, FEM analysis, Slip Slope, ABS.

1. INTRODUCTION

As a result of the recall of Bridgestone/Firestone tires in 2000, the US Transportation Recall Enhancement, Accountability, and Documentation (TREAD) legislation mandated that every new automobile be equipped with a Tire Pressure Monitoring System (TPMSs) [1, 2]. The TPMS employs pressure or other types of sensor and a reliable method of transferring the data from inside a pneumatic tire to alert drivers when tires are under-inflated [3, 4]. This legislation has given impetus to the development of advanced tire technologies.

In Europe, the European Transport Safety Council's (ETSC) general reports on EU fatalities illustrate that each year 42 000 EU citizens are killed and over 3.5 million injured in traffic accidents. According to a report from the German Traffic Safety Committee, more than half of accidents involving personal injury are caused by slippery surfaces due to rain, ice or snow. Every year, 40 people are killed in Germany and over 2 000 injured due to defective tires alone [5].

A survey by the APPOLO project revealed that disseminating information about adverse road conditions to in-vehicle applications, drivers and other road users has considerable potential in preventing or reducing the impact of accidents. The decrease in the number of fatalities, provided that the entire automobile fleet is equipped with intelligent tire systems, could, according to conservative estimates, be at least 10%. This means that every year over 4 000 lives could be save in EU countries [6].

Various reports clearly show that adverse road conditions and tire defects play a major role in road traffic accidents. As a consequence, there is an urgent need, from a traffic safety point-of-view, for intelligent tires with a road condition warning system to optimize control on poor surfaces, a tire defect detection system and a TPMS. Intelligent tires, equipped with sensors for monitoring applied strain [7, 8] are effective in improving reliability and control systems, such as anti-lock braking systems (ABSs) [9-12].

The key factors for intelligent tire sensors are: 1) development of a direct tire deformation or strain measurement system with sufficiently low stiffness and high elongation for practical application; 2) development of a wireless communication system between tires and vehicle that operates without a battery; 3) demonstration of the use model of strain data for improved safety and comfort as well as providing additional features that can be used in other aspects of automotive safety and design.

In previous studies [13, 14], we developed two types of strain sensors using changes in capacitance. The first is a patch-type sensor using a relatively soft material so that the sensor does not interfere with tire deformation and avoids debonding, which is difficult. The second is a self-sensing method using the tire structure itself as the sensor. This has the advantage that an attached sensor is not needed and debonding problems are eliminated.

We have also developed a battery-less wireless communication system composed of a tuning circuit, external transmitter and external receiver [15]. Since the tuning circuit acts as a frequency filter, the tuning frequency of the sensor can be wirelessly measured, without use of batteries in the sensor circuit. The proposed technologies are applied to radial automobile tires and compression tests performed. Experimental results demonstrate that the method is effective for passive, wireless strain monitoring. However, a specific model of strain use for improved tire safety has not been presented as yet; hence, a model is urgently needed.

In this study, we demonstrate a use model of measured strain data for an optimized braking control and road condition warning system. Relationships between strain sensor outputs and tire mechanical parameters, including braking torque, effective radius and contact patch length, are calculated using finite element analysis. Optimized braking control and road condition warning systems based on strain data are suggested.

2. SLIP SLOPE CURVE

First, we investigate the relationship between strain data obtained from the proposed sensors and tire configurations, such as effective radius, contact patch length and braking torques. Effective radius is the key parameter in that it enables one to estimate the slip ratio of tires. There are several ways to define slip ratio [16, 17], but this thesis adopts the global definition used by the Society of Automotive Engineers (SAE) to describe the ABS mechanism. SAE defines slip ratio as:

$$\vartheta = \frac{V_s}{V} = \frac{V - \omega r_e}{V}, \tag{1}$$

where V_s is tire slip speed, ω tire angular velocity, r_e effective rolling radius and V vehicle (or tire) absolute velocity. The absolute velocity of a driven wheel is computed from the velocities of the two non-driven wheels and geometric relations in a straightforward manner:

$$\vartheta = 1 - \frac{\omega r_e}{\omega_f r_f}, \tag{2}$$

where r_f and ω_f are the radius and angular velocity of a free rolling tire, respectively.

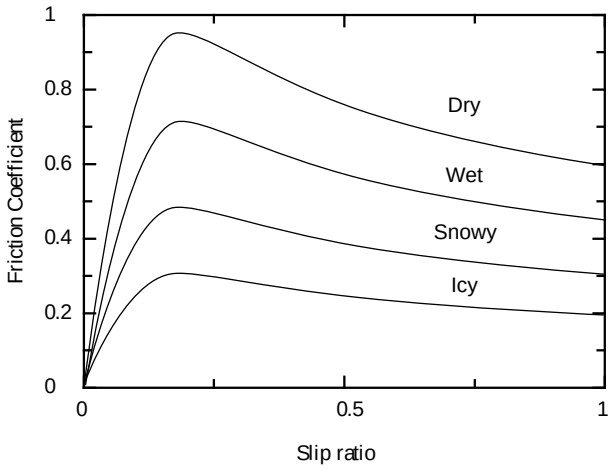

Fig. 1 Schematic of slip slope curve: wheel slip versus friction coefficient ratio for various road conditions: dry, wet, snowy and icy.

The friction coefficient μ is defined by the normal force (wheel load), F_{N}, divided by the longitudinal tire force (driving or braking force), F_{t}:

$$\mu = \frac{F_{\mathrm{t}}}{F_{\mathrm{N}}}. \tag{3}$$

The slip ratio becomes positive where the tractive force F_x is positive and negative where the force is negative. From Eq. (1), slip ratio, ϑ, becomes 1 when the tire is completely locked (i.e. ω=0), while a zero slip ratio indicates perfect rolling without slipping. Figure 1 shows a typical curve of frictional coefficient versus slip ratio[18]. It can be seen from the curve that the peak friction coefficient occurs at a slip ratio equal to 0.15, regardless of road conditions (dry, wet, snowy or icy). Therefore, driving and braking with the slip ratio constant at 0.15 produces optimal tire control with maximum driving and braking torque. Referring to the definition of slip ratio in Eq. (1), 0.15 slip ratio can be obtained numerically by specifying the tire slip velocity $V_{\mathrm{s}} = r_{\mathrm{e}}\omega$, such that it becomes 85% of the vehicle (or tire) velocity V. Since the effective rolling radius r_{e} serves as an alternative measure of slip ratio in a rolling tire, effective radius measurements can be used to achieve optimal control with maximum braking torque.

FEM analysis is used in this study on tire deformation under various wheel loads and braking torques, and the relationship between strain distribution along the sensor sampling point, circumferential strain at the center of the inner tire surface and tire configurations are calculated. Since driving and braking torques alter strain distribution between the tire contact points, they are also estimated using the strain sensor. Thus, the effects of braking torque on the strain distribution of the tire are investigated. Finally, we address the use model of the strain data from the proposed tire sensor for improving tire safety.

3. OPTIMIZATION OF BRAKING AND DRIVING CONTROL USING STRAIN DATA

3-1 Finite element analysis

To examine the relationship between tire strain distribution and other tire properties, such as effective length, braking torque, etc., calculations are performed using the FEM application program, ANSYS ver. 10. A representative automobile tire 195/60R14 is considered. Figures 2 (a) and (b)

show the three-dimensional FEM model, where ANSYS elements SOLID186, TARGET170, CONTACT174 and MPC184 elements are employed.

SOLID186 is a 3-D 20-node solid element that exhibits quadratic displacement behavior. CONTACT174 is a 3-D 8-node surface-to-surface contact element, which is used to represent contact and sliding between 3-D "target" surfaces (TARGET170) and a deformable surface, defined by this element. The contact elements themselves overlay the solid elements describing the boundary of a deformable body and can be in contact with the target surface, defined by TARGET170. The MPC184 element restricts the kinematic constraints at the rim nodes and represents the wheel loads and braking torque. The total number of elements is 4904 and there are 20 823 nodes.

Modern pneumatic tires consist of a specific combination of rubber compounds, cord and steel belts. The main components are the body, sidewall, beads and tread. The finite element model developed by Holscher *et al*. [19] is used as a reference for set-up. The simulation procedure includes the following features:

Specific behavior of rubber: Rubber shows a nonlinear stress–strain relationship and, is also incompressible. This behavior is well described by the Mooney–Rivlin function, with the strain-energy density function W defined by [17]:

$$W(J_1, J_2, J_3) = C_{10}(J_1 - 3) + C_{01}(J_2 - 3) + \frac{1}{D_1}(J_3 - 1)^2, \tag{4}$$

where C_{01} and C_{10} are material constants characterizing the deviatoric deformation of the material and are determined experimentally. D_1 is the parameter associated with material incompressibility, and J_1, J_2, and J_3 are invariants of the Green–Lagrangian strain tensor. Three material constants are related to the shear modulus τ and the bulk modulus κ as follows:

$$C_{10} + C_{01} = \frac{\tau}{2}, \tag{5}$$

$$D_1 = 2\kappa. \tag{6}$$

From this, one can derive the next relation for determining the Poisson ratio:

$$v = \frac{3\kappa/\tau - 2}{6\kappa/\tau + 2}, \tag{7}$$

$$\frac{\kappa}{\tau} = \frac{D_1}{4(C_{10} + C_{01})}. \tag{8}$$

Since v approaches 0.5 as D_1 increases for a given C_{10} and C_{01}, the incompressibility of rubber-like hyperelastic materials can be asymptotically enforced. The Mooney constants used are listed Table 1 [19, 20].

Constant inflation pressure: Inflation pressure produces a force perpendicular to the tire inner surface. This effect is well described by the pressure option in ANSYS: a constant surface force is added to every element at the inner surface of the tire and the direction of this force is kept perpendicular to the surface during each solution increment. An inflation pressure of 200 kPa is adopted in the finite element analysis.

Coulomb friction between tire and road: Tire road contact tire complicates the finite element model since contact and friction problems are highly nonlinear. The contact problem in the FEM model is described by the application of a deformable body (tire) to a rigid body (road). The friction is modeled by an algorithm in ANSYS; the friction coefficient between tire and road is set to 0.3.

Tire rotation: Tire rotation is modeled by a discrete portion of the rim for each increment.

Symmetry: It is assumed that the tire rolls straight and forward along the roadway so there are no additional lateral forces. Therefore, the tire is considered to be symmetrical and only one half is modeled with the finite element model. The nodes at the symmetry line are perpendicularly fixed to it.

The major numerical difficulties in the analysis are the geometric non-linearities due to the large deformations, the incompressibility of elastomers and the specific boundary conditions of the contact between tire and road. Since these increase simulation running time, the finite element tire model is simplified in that the composite structure, including the bead wire or steel belt layer, are modeled as three different material parts: tread, shoulder, bead, so that simulations can be calculated in a realistic time.

Since the tire is strongly deformed in the contact area between tire and road, more elements must be used in this region. To obtain a finer grid in the contact areas, the tire is split into sections with elements of different size and angle. The sector in contact with the road contains elements covering 1.25° of the tire circumference. The angle of the other sector is 5° since this part of the tire is only slightly deformed.

An external force can be included in the analysis by the introduction of a special node, from now on referred to as the central node (C_n) [21, 22]. This node belongs to no finite element and its coordinates are (0, 0) (see Fig. 3). The degrees of freedom of each bead node are constrained to be dependent on the degrees of freedom of the central node with a multipoint constraint element MPC184 in ANSYS. First, a numerical analysis is carried by applying internal pressure and vertical wheel loads statically using the central node (Fig. 3). After a nonlinear calculation with air pressure and vertical wheel loads, driving or braking torque is applied statically to the central node. The strain in the circumferential direction at the center of the inner surface of the tire, as shown in Fig. 2 (b), is calculated and the relationship between the obtained strain and tire deformation is considered.

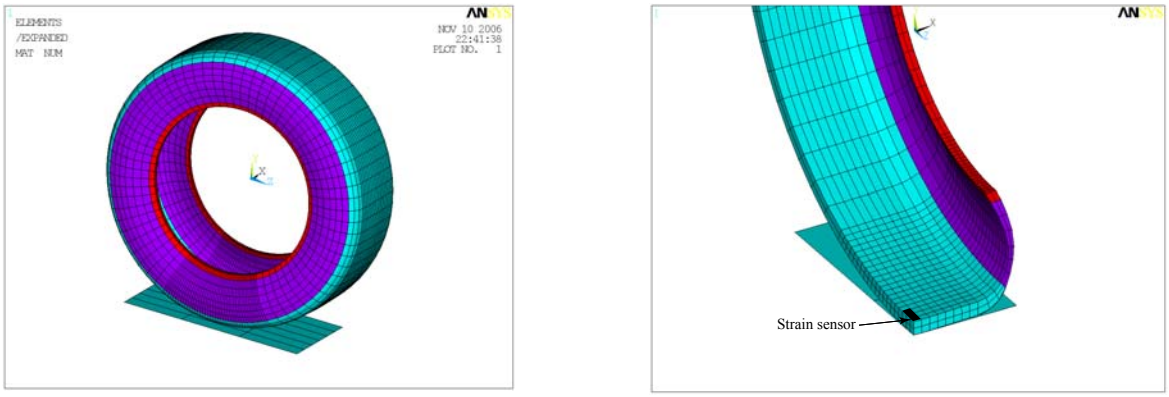

(a) (b)

Fig. 2 Finite element model of a passenger automobile tire: (a) overall view (b) contact area between tire and road surface (half and cut mode). The strain sensor is attached to the middle right on the inner surface of the tire.

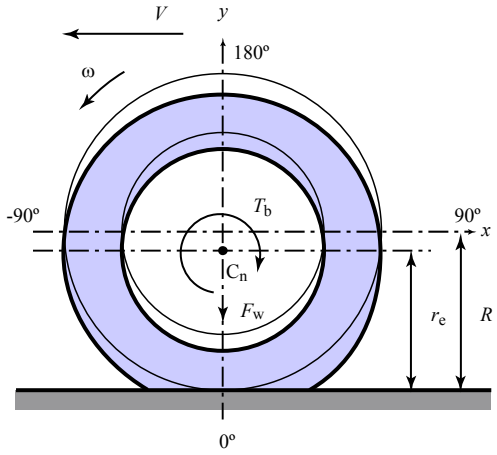

Fig. 3 Tire deformation for wheel load F_w and braking torque T_b.

Table 1 Material properties of the Mooney–Rivlin model used in the finite element analysis.

Rubber material	C_{10}	C_{01}	v
Bead filler	14.14 MPa	21.26 Mpa	0.45
Sidewall	171.8 kPa	830.3 kPa	0.45
Tread	806.1 kPa	1.805 MPa	0.45

3-2 Contact patch length and effective radius

Figure 4 shows tire configurations when various wheel loads are applied. The abscissa is x and the ordinate y, as shown in Fig. 3. The origin of the x- and y-axes is defined at the tire center under no load. As wheel load increases, contact patch length increases and the effective radius decreases. Figure 5 shows strain distributions on the inner surface of the tire when various vertical wheel loads are applied. The abscissa is the rotational angle θ, when the contact point is set to zero, as shown in Fig. 3, while the ordinate is the calculated strain at the inner surface in the circumferential direction or simulated sensor signal. As can be seen, the tensile strain occurs at the contact point, $\theta = 0$, while compressive strain occurs at the periphery of the contact point, around $\theta = \pm 10$. The tensile strain is due to bending in the circular tire at the contact point; tensile strain arises at the inner surface. Compressive strains at the periphery are due to the compressive effect from the tensile strain area. The presence of the tensile and compressive strain areas around the contact point agrees with the experimental results [23].

Morinaga *et al*. [24] proposed an estimation method for contact patch length by calculating the waveform of the time derivative of strain: two peaks of the waveform are the points with the

highest deformation speed and are the edges of the contact patch. Figure 6 shows the waveform of the time derivative of strain; the distance between two peaks corresponds to contact patch length.
The precise contact patch length can also be calculated using analytical results from the FEM. Figure 7 shows the relationship between contact patch length obtained using FEM (abscissa) and strain data (ordinate). The solid line indicates the ideal estimation and shows that there is clear relationship between contact patch lengths obtained using FEM and strain data; the estimation results (open circles) are close to the ideal estimation (solid line). Therefore, contact patch length, one of the most important indicators of tire deformation, can be estimated in service using the proposed strain sensor.

Contact patch length provides a full picture of overall tire configuration. There is also a relationship between contact patch length and effective radius. Increasing contact patch length indicates larger deformation in the tire; the center of the tire becomes lower, resulting in a reduction in the effective radius. Figure 8 shows the relationship between contact patch length and effective radius. It clarifies the negative linear relation between these two values. From the definition of slip ratio in Eq. (2), the slip ratio can be numerically calculated using the obtained effective radius.

3-3 Wheel loads

It is also found from Fig. 5 that, as the applied wheel loads increase, the compressive strain increases monotonically. Conversely, tensile strain increases up to 500 N but decreases at 1000 N. This is because the tire is in complete contact and bent at the contact point under a load of 500 N, but bending does not increase at larger wheel loads. Figure 9 shows the maximum compressive strain at various wheel loads. The abscissa is maximum compressive strain and the ordinate is wheel load. The maximum compressive strain increases as the wheel loads increase. Therefore, applied wheel load can be estimated from maximum compressive strain.

3-4 Driving and braking torques

When driving or braking torque is applied, the ratio between forward and backward compressive strains changes. Braking torque increases the compressive strain in the rear area ε_b, where the rotation angle θ is positive, and decreases the compressive strain at the forward area ε_f, as can be seen in Fig. 3. The compressive strain ratio between rear and forward areas is:

$$r_{fb} = \frac{\varepsilon_f + \varepsilon_p}{\varepsilon_b + \varepsilon_p}, \tag{9}$$

where ε_p is the strain due to inflation pressure.

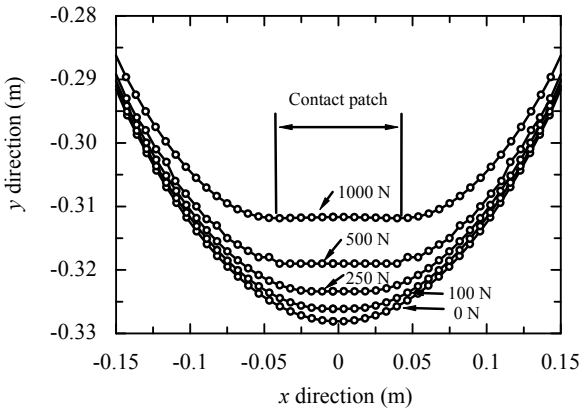

Fig. 4 Tire deformation at wheel loads of 0, 100, 250, 500 and 1000 N.

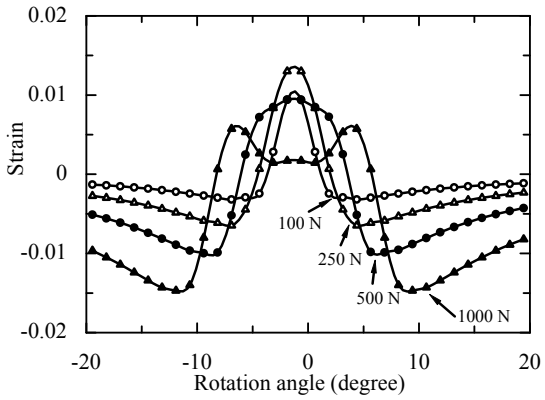

Fig. 5 Strain and rotation angle for wheel loads of 100, 250, 500 and 1000 N.

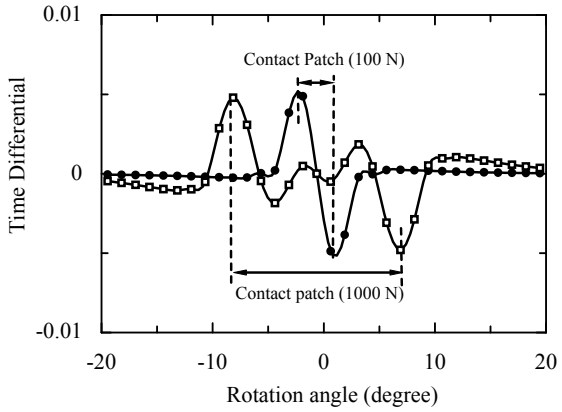

Fig. 6 Time derivative of strain for wheel loads of 100 N (●) and 1000 N (□). Two peaks of the waveform indicate the edges of the contact patch.

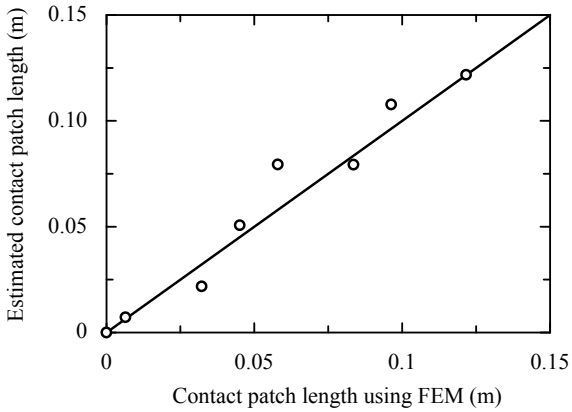

Fig. 7 Relationship between contact patch lengths obtained using FEM and estimated from strain data. The solid line indicates the ideal estimation.

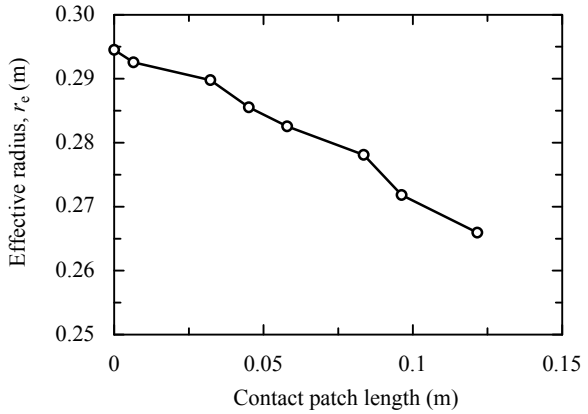

Fig. 8 Effective radius versus contact patch length obtained using strain data.

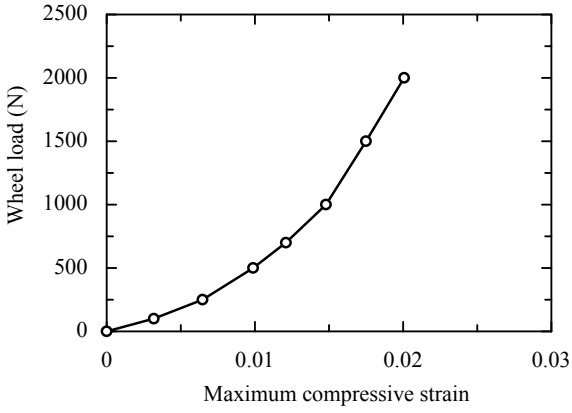

Fig. 9 Relationship between wheel load F_w and maximum compressive strain.

Figure 10 shows calculated strain variation from the sensor at braking torques of 0, 144 and 342 Nm. As braking torque increases, the backward compressive strain increases, while the forward compressive strain decreases. Figure 11 shows the ratio between the backward and forward compressive strain at the contact point, r_{fb}, due to braking torque changes. The abscissa is compressive strain ratio and the ordinate is applied braking torque. As applied torque increases, the compressive strain ratio increases linearly, which means backward strain decreases (or compressive

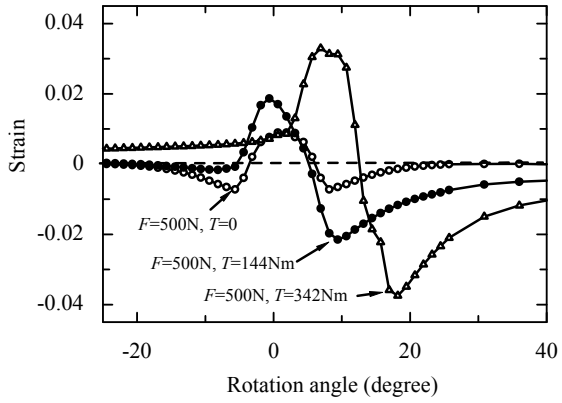

Fig. 10 Strain distribution when braking torque is applied at 0, 144 and 342 Nm. Wheel load F_w is set to 500 N.

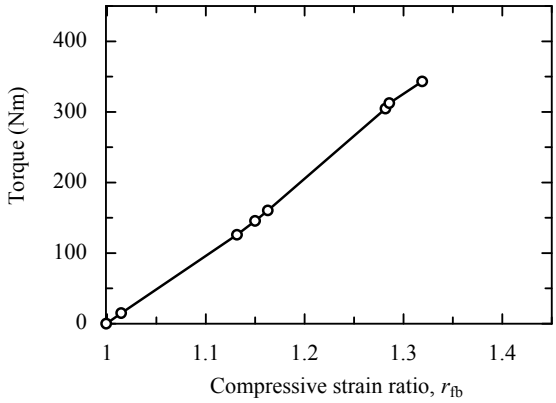

Fig. 11 Compressive strain ratio r_{fb} versus applied braking torque T_b.

strain increases) and forward strain increases. Therefore, braking torque can also be obtained from the compressive strain ratio obtained from the strain curve of the sensor.

4. OPTIMIZED BRAKING CONTROL AND ROAD CONDITION WARNING SYSTEMS

Figure 12 shows a schematic illustration of the proposed intelligent tire system including the sensing [14, 23] and wireless transmission [13, 15, 25] proposed by the authors. The flexible sensor has advantages in that it is simple and easy to attach to existing tires. The self-sensing method does not suffer from sensor-debonding problems and is resilient against environmental changes. At present, the greatest problem facing the proposed system is its difficulty of manufacture as the method uses steel wires completely embedded inside the tire. Since it is necessary to connect the steel wires to a wireless communication circuit, the current tire-manufacturing process would have to be altered to implement this system. However, production methods for intelligent tires have been proposed in which a monitoring device is embedded inside the tire during manufacture [26]. As for wireless transmission, wireless communication using tuning frequency is preferable in that it is: battery-less, has a high sampling frequency, low cost and is practical to manufacture.

Using the ratio between braking or driving torque and wheel loads, the friction coefficient between the tire and road surface can be measured. Using the friction coefficient and slip ratio obtained from effective radius measurements, one can represent the slip ratio and friction curve (slip slope curve), as shown in Fig. 1. Measurements of the slip slope curve enable optimization of vehicle control by maintaining a constant slip ratio at the maximum friction coefficient. Implementation of a road condition warning system is also a possibility. Such a system would warn a driver if the recorded friction coefficient at a certain slip ratio is lower than a reference value previously measured under dry road conditions.

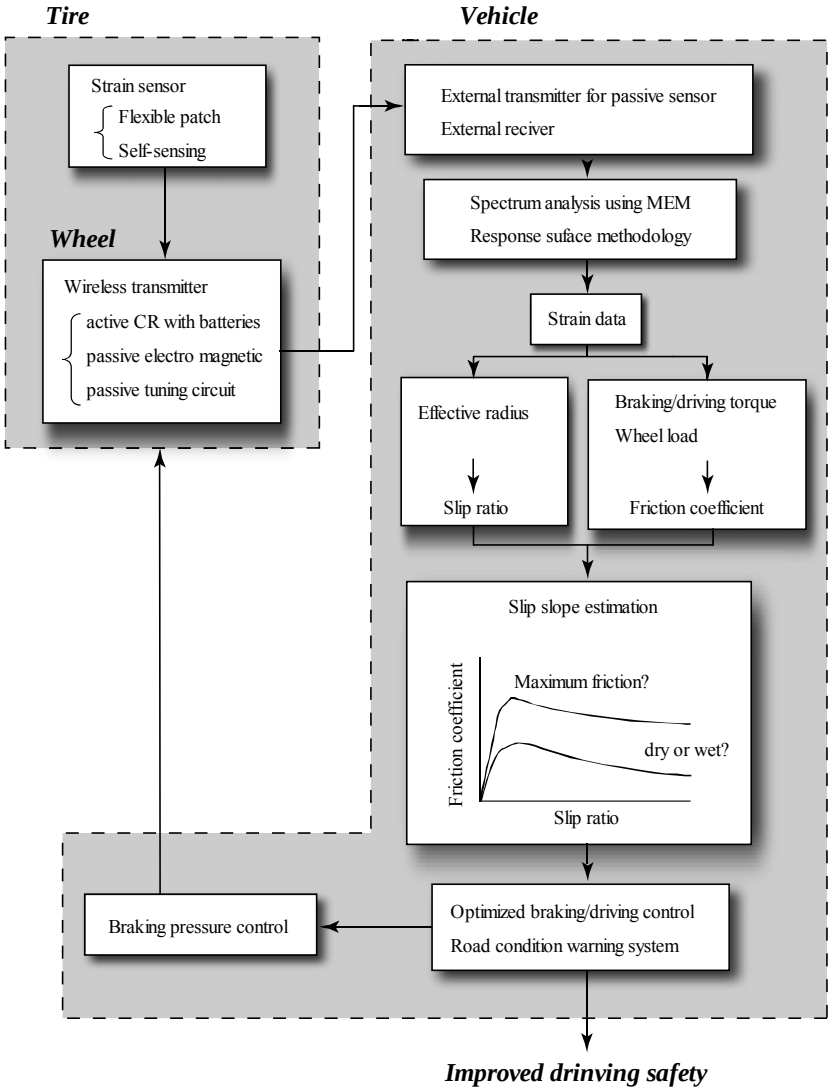

Fig. 12 Schematic illustration of optimized braking control and road condition warning systems.

5. CONCLUSIONS

We investigated the relationship between variations in strain on the inner surface of pneumatic tires and mechanical parameters including, contact patch length, effective radius, wheel load and braking torque. The calculations were carried out using finite element analysis and simulate the strain sensor signal when a tire rotates. The following results were obtained:

1. Contact patch length is estimated using the distance between two time derivative peaks in the strain data. The contact patch length provides the effective radius and in turn the slip ratio.
2. Wheel load can be estimated using maximum compressive strain and braking torque using the compressive strain ratio. The friction coefficient can be obtained from the ratio of those two values.
3. It is suggested that optimized braking control and road condition warning systems use strain data. Braking control is optimized by keeping the slip ratio constant. A road condition warning system could be actuated if the recorded friction coefficient at a certain slip ratio fell below a reference value for safe road conditions.

REFERENCES

1. Title 49 United States Code 30101, Transportation Recall Enhancement, Accountability, and Documentation (TREAD) Act, Public Law 106-414-NOV.1, 106th Congress, US, (2000).
2. National Highway Traffic Safety Administration, Federal motor vehicle safety standards; tire pressure monitoring systems; controls and displays, NHTSA-2000-8572, (2000).
3. Yamagiwa, T., M. Orita, and T. Harada, Development of a tire pressure monitoring system for motorcycles, JSAE Review, **23**, (2003) pp.495-496.
4. Garrott, W.R. and G.J. Forkenbrock, Testing the effects of tire pressure monitoring system minimum activation pressure on the handling and rollover resistance of a 15-passenger van, DOT HS 809 701, (2004).
5. European Transport Safety Council, Road accident data in the enlarged european union, (2006).
6. Technical Research Centre of Finland (VTT), Intelligent tyre systems - state of the art and potential technologies, APOLLO IST-2001-34372 Intelligent tyre for accident-free traffic, Deliverable D7, (2001).
7. Sergio, M., et al. *On road tire deformation measurement system using capacitive-resistive sensor*. in *Proceedings of Second IEEE International Conference on Sensors: IEEE Sensors 2003*. 2003. Tronto, Ont. Canada.
8. Magori, V., V.R. Magori, and N. Seitz. *On-line determination of tyre deformation, a novel sensor principle*. in *IEEE Proceedings of Ultrasonics Symposium* 1998. Sendai, Japan.
9. Palmer, M.E., et al., Wireless smart tires for road friction measurement and self state determination, 43rd AIAA/ASME/ASCE/AHS Structures, Structural Dynamics, and Materials Conference **AIAA-2002-1548**, (2002) pp.
10. Todoroki, A., S. Miyatani, and Y. Shimamura, Wireless strain monitoring using electrical capacitance change of tire: part I - with oscillating circuit, Smart Materials and Structures, **12**, (2003) pp.403-409.
11. Todoroki, A., S. Miyatani, and Y. Shimamura, Wireless strain monitoring using electrical capacitance change of tire: part II - passive, Smart Materials and Structures, **12**, (2003) pp.410-416.
12. Li, L., F.-Y. Wang, and Q. Zhou, Integrated longitudinal and lateral tire/road friction modeling and monitoring for vehicle motion control, IEEE transactions on Intelligent Transportation Systems, **7**(1), (2006) pp.1-19.
13. Matsuzaki, R. and A. Todoroki, Passive wireless strain monitoring of actual tire using capacitance-resistance change and multiple spectral features, Sensors and Actuators A, **126**(2), (2005) pp.277-286.
14. Matsuzaki, R. and A. Todoroki, Wireless flexible capacitive sensor based on ultra-flexible epoxy resin for strain measurement of automobile tires, Sensors and Actuators A, **140**, (2007) pp.32-42.
15. Matsuzaki, R. and A. Todoroki, Passive wireless strain monitoring of tyres using capacitance and tuning frequency changes, Smart Materials and Structures, **14**, (2005) pp.561-568.
16. Mauer, G.F., A fuzzy logic controller for an ABS braking system, IEEE Transactions on Fuzzy Systems, **3**(4), (1995) pp.381-388.
17. Cho, J.R., et al., Estimation of dry road braking distance considering frictional energy of patterned tires, Finite Elements in Analysis and Design, **42**(14-15), (2006) pp.1248-1257.
18. Lee, C., K. Hedrick, and K. Yi, Real-time slip-based estimation of maximum tire-road friction coefficient, IEEE/ASME Transactions on Mechatronics, **9**(2), (2004) pp.454-458.
19. Holscher, H., et al., Modeling of pneumatic tires by a finite element model for the development of a tire friction remote sensor, caesar-smm, (2004) pp.40.

20. Tonuk, E. and Y.S. Unlusoy, Prediction of automobile tire cornering force characteristics by finite element modeling and analysis, Computers and Structures, **79**, (2001) pp.1219-1232.
21. Pelc, J. *Static three-dimensional modelling of pneumatic tyres using the technique of element overlaying*. in *Proceedings of the Institution of Mechanical Engineers, Part D: Journal of Automobile Engineering*. 2002.
22. Pelc, J., Towards realistic simulation of deformations and stresses in pneumatic tyres, Applied Mathematical Modelling, **31**, (2007) pp.530-540.
23. Matsuzaki, R. and A. Todoroki, Wireless strain monitoring of tires using electrical capacitance changes with an oscillating circuit, Sensors and Actuators A, **119**(2), (2005) pp.323-331.
24. Morinaga, H., et al. *The possibility of intelligent tire (technology of contact area information sensing)*. in *31st FISITA Automotive Congress*. 2006. Ykohama, Japan.
25. Matsuzaki, R., et al., Passive wireless strain monitoring of a tire using capacitance and electromagnetic induction change, Advanced Composite Materials, **14**(2), (2005) pp.147-164.
26. Koch, R.W., et al., *Method for embedding a monitoring device within a tire during manufacture*. 1994, Bridgestone/Firestone, Inc.